Inorg. Chem. **2004**, *43*, 506–514

EPR and Magnetic Properties of Heteronuclear $Mn_nMg_{6-n}(O_2CNEt_2)_{12}$: Impact of Structural Distortions on Mn(II) in Weak Ligand Fields

M. Tyler Caudle,*,† Charles. K. Mobley,† Laura M. Bafaro,† Russell LoBrutto,‡ Gordon T. Yee,§ and Thomas L. Groy†

Department of Chemistry and Biochemistry, Arizona State University, Tempe, Arizona 85287-1604, School of Life Sciences, Arizona State University, Tempe, Arizona 85287-1601, and Department of Chemistry, Virginia Polytechnic Institute and State University, Blacksburg, Virginia 24061-0212

Received August 15, 2003

The reaction between Mn_6L_{12} and Mg_6L_{12} (L = *N*,*N*-diethylcarbamate) results in isolation of heteronuclear complexes $Mn_nMg_{6-n}L_{12}$. A series was prepared with different doping factors *n* by varying the Mn/Mg ratio in the crystallization solutions. Single-crystal X-ray diffraction shows that $MnMg_5L_{12}$ is isostructural with Mn_6L_{12} and Mg_6L_{12}. Magnetic susceptibility data on the series $Mn_nMg_{6-n}L_{12}$ (n = 1–6) are consistent with antiferromagnetic Mn···Mn interactions. At low *n*, the magnetic data demonstrate the formation of magnetically isolated Mn^{2+} centers. This was confirmed by measurement of the EPR spectrum at a doping factor $n = 0.06$ in solution, as a powder, and as single crystals. These show hyperfine interactions consistent with isolated Mn^{2+}. The EPR spectrum of $Mn_{0.06}Mg_{5.94}L_{12}$ exhibits a dominant signal at $g_{eff} = 4$, and a wide series of less intense signals spanning 200–6000 G in the X-band regime. This unusual behavior in a weak-field Mn^{2+} complex is attributed to the substantial distortions from cubic ligand field geometry in this system. The $g_{eff} = 4$ signals are attributed to a C_2-symmetric hexacoordinate Mn^{2+} ion with $D > 0.3$ cm^{-1} and $E/D = 0.33$. The wide series is assigned to an axial C_{4v} pentacoordinate Mn^{2+} site with $D = 0.05$ cm^{-1}. Comparison of the $g_{eff} = 4$ signals to the $g = 4.1$ signals exhibited by the tetramanganese complex in photosystem II belies the fact that they almost certainly arise from different spin systems. In addition, the similarity of the spectrum of $Mn_nMg_{6-n}L_{12}$ to mononuclear Mn^{4+} complexes suggests that considerable care must be exercised in the use of EPR as a fingerprint for the manganese oxidation state, particularly in manganese proteins where molecular composition may not be precisely established.

Introduction

The electron spin properties of manganese have long been of interest as a spectroscopic probe of manganese centers in manganese proteins[1−10] and as a spectroscopically active surrogate for other divalent metal ions.[11] The Mn(II) (S = 5/2) and Mn(IV) (S = 3/2) oxidation states possess Kramer's ground-state doublets and exhibit characteristic spin transitions in the normal mode X-band regime. The Mn(III) state (S = 2) has four unpaired electrons and typically exhibits a pronounced Jahn−Teller distortion, which results in substantial spin−orbit coupling. As a result, mononuclear Mn(III) centers are typically silent in the normal mode ($H_1 \perp H_0$) regime, although they do show spin transitions when measurements are made in the parallel mode ($H_1 \parallel H_0$) regime.[12]

* Author to whom correspondence should be addressed. E-mail: tcaudle@asu.edu.
† Department of Chemistry and Biochemistry, Arizona State University.
‡ School of Life Sciences, Arizona State University.
§ Virginia Polytechnic Institute and State University.

(1) Ubbink, M.; Worrall, J. A. R.; Canters, G. W.; Groenen, E. J. J.; Huber, M. *Annu. Rev. Biophys. Biomol. Struct.* **2002**, *31*, 393−422.
(2) Carmieli, R.; Manikandan, P.; Epel, B.; Kalb, A. J.; Schnegg, A.; Savitsky, A.; Moebius, K.; Goldfarb, D. *Biochemistry* **2003**, *42*, 7863−7870. Petrescu, A. L.; Georgescu, R.; Rotaru, M.; Lehaci, F.; Petrescu, S. M. *Stud. Cercet. Biochim.* **1992**, *35*, 101−108. Antanaitis, B. C.; Brown, R. D., III; Chasteen, N. D.; Freedman, J. H.; Koenig, S. H.; Lilienthal, H. R.; Peisach, J.; Brewer, C. F. *Biochemistry* **1987**, *26*, 7932−7937. Meirovitch, E.; Luz, Z.; Kalb, A. J. *J. Am. Chem. Soc.* **1974**, *96*, 7538−7542. Meirovitch, E.; Luz, Z.; Kalb, A. J. *J. Am. Chem. Soc.* **1974**, *96*, 7542−7546. Von Goldammer, E.; Zorn, H. *Eur. J. Biochem.* **1974**, *44*, 195−199. Reed, G. H.; Cohn, M. *J. Biol. Chem.* **1970**, *245*, 662−664. Nicolau, C.; Kalb, A. J.; Yariv, J. *Biochim. Biophys. Acta* **1969**, *194*, 71−73.
(3) Bogumil, R.; Kappl, R.; Huettermann, J.; Witzel, H. *Biochemistry* **1997**, *36*, 2345−2352. Bogumil, R.; Kappl, R.; Huettermann, J.; Sudfeldt, C.; Witzel, H. *Eur. J. Biochem.* **1993**, *213*, 1185−1192.
(4) Whiting, A. K.; Boldt, Y. R.; Hendrich, M. P.; Wackett, L. P.; Que, L., Jr. *Biochemistry* **1996**, *35*, 160−170.

10.1021/ic0349757 CCC: $27.50
Published on Web 12/23/2003

In weak ligand fields, Mn(II) centers give a single transition at $g_{eff} \approx 2$, which is split into six hyperfine lines by the ^{55}Mn nuclear spin ($I = 5/2$). However, simple spectra of this type are indicative of a cubic ligand field where the zero-field splitting parameter D is negligible and all of the $\Delta M_s = \pm 1$ transitions are degenerate as a result. For a small but finite value for D, the degeneracy is removed and the spectrum exhibits 5-fold fine structure.[13] In more strongly axial systems where D is comparable to $h\nu$, high-spin d^5 ions such as Mn^{2+} and Fe^{3+} often exhibit tetragonal spectra with $g_\perp \approx 6$ and $g_{||} = 2$, a situation observed for many porphyrin, phthalocyanin, and related complexes of Mn^{2+}.[14−16] Ligand fields of lower symmetry are often characterized by a rhombic signal at $g_{eff} = 4.3$, but this is typically observed for relatively strong field ligands.[15,17] Interestingly, Mn^{4+} complexes, which have a d^3 configuration with $S = 3/2$, also often exhibit signals between $g_{eff} = 4$ and $g_{eff} = 5$.[18] The variety of EPR signals exhibited by Mn^{2+} in different coordination environments and their similarity to other spin systems mean that EPR spectra could be mistakenly assigned to manganese in an incorrect oxidation state if care is not taken to obtain corroborating evidence. General assignment of the manganese oxidation state therefore requires that the electron spin properties of Mn(II) in unusual ligand field environments be fully understood. There are a number of examples of molecular mononuclear Mn(II) centers in weak-field environments whose EPR spectra have been analyzed,[19,20] but these tend to involve small structural distortions that lead to small perturbations of the Zeeman terms. This restriction is true of Mn^{2+}-doped metal halides and oxides as well.[21,22] There are relatively few examples of molecular Mn^{2+} centers in weak-field environments that are highly distorted from idealized geometries.

We recently reported the preparation of a series of polyheteronuclear coordination compounds of the general form $Co_nMg_{6-n}L_{12}$[23] (L = *N*,*N*-diethylcarbamate), in which a hexanuclear core is supported by 12 diethylcarbamato anions. These were prepared by simply mixing the homonuclear derivatives Co_6L_{12} and Mg_6L_{12} in solution and recrystallizing, which resulted in scrambling of the Co^{2+} and Mg^{2+} ions between complexes. The Co^{2+} doping factor n was controlled by the stoichiometry of the solution. The M_6L_{12} motif is unique in having pentacoordinate and hexacoordinate sites for the metal ions that are both distorted from idealized geometries.[24,25] For $n \leq 3$, the Co^{2+} ions reside exclusively in the pentacoordinate sites of the M_6L_{12}

(5) Un, S.; Dorlet, P.; Voyard, G.; Tabares, L. C.; Cortez, N. *J. Am. Chem. Soc.* **2001**, *123*, 10123−10124. Schwartz, A. L.; Yikilmaz, E.; Vance, C. K.; Vathyam, S.; Koder, R. L.; Miller, A-F. *J. Inorg. Biochem.* **2000**, *80*, 247−256. Song, C.-H.; Park, E-K.; Suh, H. J.; Lee, Y. S.; Choi, J. W.; Ra, K. S. *J. Microbiol. Biotechnol.* **1999**, *9*, 271−275. Campbell, K. A.; Yikilmaz, E.; Grant, C. V.; Gregor, W.; Miller, A-F.; Britt, R. D. *J. Am. Chem. Soc.* **1999**, *121*, 4714−4715. Hsieh, Y.; Guan, Y.; Tu, C.; Bratt, P. J.; Angerhofer, A.; Lepock, J. R.; Hickey, M. J.; Tainer, J. A.; Nick, H. S.; Silverman, D. N. *Biochemistry* **1998**, *37*, 4731−4739. Peterson, J.; Fee, J. A.; Day, E. P. *Biochim. Biophys. Acta* **1991**, *1079*, 161−168. Whittaker, J. W.; Whittaker, M. M. *J. Am. Chem. Soc.* **1991**, *113*, 5528−5540.

(6) Sossong, T. M., Jr.; Khangulov, S. V.; Cavalli, R. C.; Soprano, D. R.; Dismukes, G. C.; Ash, D. E. *J. Biol. Inorg. Chem.* **1997**, *2*, 433−443. Reczkowski, R. S.; Ash, D. E. *J. Am. Chem. Soc.* **1992**, *114*, 10992−10994.

(7) Dismukes, G. C. *Chem. Rev.* **1996**, *96*, 2909−2926.

(8) Meier, A. E.; Whittaker, M. M.; Whittaker, J. W. *Biochemistry* **1996**, *35*, 348−360. Zheng, M.; Khangulov, S. V.; Dismukes, G. C.; Barynin, V. V. *Inorg. Chem.* **1994**, *33*, 382−387. Khangulov, S. V.; Barynin, V. V.; Voevodskaya, N. V.; Grebenko, A. I. *Biochim. Biophys. Acta* **1990**, *1020*, 305−310. Khangulov, S. V.; Gol'dfel'd, M. G.; Gerasimenko, V. V.; Andreeva, N. E.; Barynin, V. V.; Grebenko, A. I. *J. Inorg. Biochem.* **1990**, *40*, 279−292. Khangulov, S. V.; Voevodskaya, N. V.; Barynin, V. V.; Grebenko, A. I.; Melik-Adamyan, V. R. *Biofizika* **1987**, *32*, 960−966.

(9) Peloquin, J. M.; Britt, R. D. *Biochim. Biophys. Acta* **2001**, *1503*, 96−111. Ahrling, K. A.; Styring, S. *Probing Photosynth.* **2000**, 148−163.

(10) Carrell, T. G.; Tyryshkin, A. M.; Dismukes, G. C. *J. Biol. Inorg. Chem.* **2002**, *7*, 2−22.

(11) Reed, G. H.; Poyner, R. R. *Met. Ions Biol. Syst.* **2000**, *37*, 183−207. Feig, A. L. *Met. Ions Biol. Syst.* **2000**, *37*, 157−182.

(12) Campbell, K. A.; Lashley, M. R.; Wyatt, J. K.; Nantz, M. H.; Britt, R. D. *J. Am. Chem. Soc.* **2001**, *123*, 5710−5719.

(13) Wertz, J. E.; Bolton, J. R. *Electron Spin Resonance. Elementary Theory and Practical Applications*; Chapman and Hall: New York, 1986.

(14) Sievertsen, S.; Moubaraki, B.; Murray, K. S.; Homborg, H. *Z. Anorg. Allg. Chem.* **1994**, *620*, 682−690. Masuya, F.; Hori, H. *Biochim. Biophys. Acta* **1993**, *1203*, 99−103. Rao, R.; Symons, M. C. R.; Harriman, A. *J. Chem. Soc., Faraday Trans.* **1982**, *78*, 3393−3396. Yonetani, T.; Drott, H. R.; Leigh, J. S., Jr.; Reed, G. H.; Waterman, M. R.; Asakura, T. *J. Biol. Chem.* **1970**, *245*, 2998−3003. Dowsing, R. D.; Gibson, J. F.; Goodgame, M.; Hayward, P. J. *J. Chem. Soc. A* **1969**, 187−193.

(15) Dowsing, R. D.; Gibson, J. F.; Goodgame, D. M. L.; Goodgame, M.; Hayward, P. J. *Nature* **1968**, *219*, 1037−1038.

(16) Dowsing, R. D.; Nieuwenhuijse, B.; Reedijk, J. *Inorg. Chim. Acta* **1971**, *5*, 301−304. Dowsing, R. D.; Gibson, J. F.; Goodgame, M.; Hayward, P. J. *J. Chem. Soc. A* **1970**, 1133−1138.

(17) Dowsing, R. D.; Gibson, J. F.; Goodgame, D. M. L.; Goodgame, M.; Hayward, P. J. *J. Chem. Soc. A* **1969**, 1242−1248.

(18) Hartman, J. R.; Foxman, B. M.; Cooper, S. R. *Inorg. Chem.* **1984**, *23*, 1381−1387. Kessissoglou, D. P.; Li, X.; Butler, W. M.; Pecoraro, V. L. *Inorg. Chem.* **1987**, *26*, 2487−2492. Chan, M. K.; Armstrong, W. H. *Inorg. Chem.* **1989**, *28*, 3777−3779. Li, X.; Lah, M. S.; Pecoraro, V. L. *Acta Crystallogr., Sect. C: Cryst. Struct. Commun.* **1989**, *C45*, 1517−1519. Chandra, S. K.; Basu, P.; Ray, D.; Pal, S.; Chakravorty, A. *Inorg. Chem.* **1990**, *29*, 2423−2428. Dutta, S.; Basu, P.; Chakravorty, A. *Inorg. Chem.* **1991**, *30*, 4031−4037. Saadeh, S. M.; Lah, M. S.; Pecoraro, V. L. *Inorg. Chem.* **1991**, *30*, 8−15. Chandra, S. K.; Chakravorty, A. *Inorg. Chem.* **1992**, *31*, 760−765. Mukhopadhyay, R.; Chatterjee, A. B.; Bhattacharyya, R. *Polyhedron* **1992**, *11*, 1353−1358. Das, G.; Bharadwaj, P. K.; Ghosh, D.; Chaudhuri, B.; Banerjee, R. *Chem. Commun.* **2001**, 323−324. Rajendiran, T. M.; Kampf, J. W.; Pecoraro, V. L. *Inorg. Chim. Acta* **2002**, *339*, 497−502.

(19) Wood, R. M.; Stucker, D. M.; Jones, L. M.; Lynch, W. B.; Misra, S. K.; Freed, J. H. *Inorg. Chem.* **1999**, *38*, 5384−5388. Heming, M.; Remme, S.; Lehmann, G. *J. Magn. Reson.* **1986**, *69*, 134−143. Goodgame, D. M. L.; El Mkami, H.; Smith, G. M.; Zhao, J. P.; McInnes, E. J. L. *J. Chem. Soc., Dalton Trans.* **2003**, 34−35. Goodgame, M.; Hussain, I. *Inorg. Chim. Acta* **1990**, *174*, 245−248. Srinivas, D.; Subramanian, S. *Cryst. Lattice Defects Amorphous Mater.* **1987**, *14*, 53−61. Dayal, R. *Indian J. Phys., A* **1979**, *53A*, 514−519. Sachs, H.; Lehmann, G. *Phys. Status Solidi B* **1979**, *92*, 417−424. Birdy, R. B.; Goodgame, M. *Inorg. Chem.* **1979**, *18*, 472−475.

(20) Matzapetakis, M.; Karligiano, N.; Bino, A.; Dakanali, M.; Raptopoulou, C. P.; Tangoulis, V.; Terzis, A.; Giapintzakis, J.; Salifoglou, A. *Inorg. Chem.* **2000**, *39*, 4044−4051.

(21) Zheng, W-C.; Wu, S-Y. *Physica B* **2001**, *301*, 186−189. Zheng, W-C. *Physica B* **1997**, *233*, 125−129. Lukin, S. N.; Teslya, O. P.; Tsintsadze, G. A. *Fiz. Tverd. Tela* **1983**, *25*, 1075−1080. Bodziony, T.; Lipinski, I. E.; Kuriata, J.; Bednarski, W. *Physica B* **2001**, *299*, 70−76. Rao, P. S. *Spectrochim. Acta, Part A* **1993**, *49A*, 897−901. Di Mauro, E.; Sano, W. *J. Phys. Chem. Solids* **1987**, *48*, 29−31. Heming, M.; Lehmann, G. *Z. Naturforsch., Teil A* **1983**, *38A*, 149−153.

(22) Naidu, Y. N.; Rao, J. L.; Lakshman, S. V. J. *Solid State Commun.* **1992**, *81*, 437−442.

(23) Caudle, M. T.; Benedict, J. B.; Mobley, C. K.; Straessler, N., A.; Groy, T. L. *Inorg. Chem.* **2002**, *41*, 3183−3190.

(24) Belforte, A.; Calderazzo, F.; Zanazzi, P. F. *J. Chem. Soc., Dalton Trans.* **1988**, 2921−2927.

(25) Belli-Dell'Amico, D.; Calderazzo, F.; Giovannitti, B.; Pelizzi, G. *J. Chem. Soc., Dalton Trans.* **1984**, 647−652. Belli-Dell'Amico, D.; Calderazzo, F.; Labella, L.; Maichle-Mössmer, C.; Straehle, J. *J. Chem. Soc., Chem. Commun.* **1994**, 1555−1556.

framework, which was attributed to the crystal field preference of the d^7 ion for the lower symmetry site.

A d^5 ion such as Mn^{2+} will have no crystal field preference and is expected to reside in both sites. Furthermore, at low *n*, we expect the majority of Mn^{2+} ions to be magnetically isolated. We have now prepared the analogous series of hexanuclear compounds $Mn_nMg_{6-n}L_{12}$ doped with Mn^{2+} ions instead. In this paper we report the preparation, structure, and solid-state and solution EPR spectra and magnetic properties of these compounds, which provides the opportunity to examine the EPR properties of Mn^{2+} in highly distorted O_5 and O_6 ligand field environments.

Experimental Section

Materials and Methods. Diethylamine from Aldrich Chemical was distilled from sodium hydroxide and stored over 4 Å molecular sieves prior to use. Manganese chloride was obtained from Aldrich and dried at 200 °C for 2 days before being stored in a glovebox under nitrogen. Infrared spectroscopy showed no evidence for remaining waters of hydration. Tetrahydrofuran was distilled from sodium benzophenone ketyl and stored under nitrogen. Hexane and heptane were distilled from calcium hydride and also stored under a nitrogen atmosphere. The precursor complex Mg_6L_{12} was prepared as described previously.[26] EPR measurements were made in the perpendicular mode configuration ($H_1 \perp H_0$) in the X-band frequency region using a Bruker ELEXSYS E580 spectrometer equipped with a Bruker 4102 rectangular cavity and Oxford ESR-900 liquid helium cryostat. Magnetic susceptibility measurements were made on an MPMS-5 SQUID magnetometer located at the National Institute of Standards and Technology, Gaithersburg, MD. Elemental microanalyses were performed by the Microanalysis Laboratory at the School of Chemical Sciences, University of Illinois.

Mn_6L_{12}. This preparation is a modification of the previous literature preparation.[24] Briefly, 15.08 g (120 mmol) of anhydrous $MnCl_2$ was combined with 250 mL of hexane under an atmosphere of nitrogen. To this solution was added 50 mL (480 mmol) of diethylamine. Then the flask was purged with carbon dioxide and the mixture stirred under 1 atm of carbon dioxide for 24 h. The white insoluble diethylammonium chloride salt was removed by filtration under nitrogen. Slow evaporation of the filtrate gave 18.8 g of crude Mn_6L_{12} as large blocklike crystals. Recrystallization from hexane followed by washing with cold hexane gave 16.3 g (46% yield) of pure Mn_6L_{12}. The complex was identified by its infrared spectrum. IR (cm^{-1}, KBr pellet): 2973, 2932, 1595, 1486, 1430, 1315, 1212, 1089, 802.

$MnMg_5L_{12}$. In a representative preparation, a thick-walled pressure flask was charged with 0.51 g (0.33 mmol) of Mg_6L_{12}, 0.12 g (0.070 mmol) of Mn_6L_{12}, and about 15 mL of heptane under nitrogen. This sealed apparatus was heated to 110 °C until all of the solids had dissolved. Then the flask was slowly cooled to room temperature over the course of 2 days, which resulted in the formation of colorless blocklike crystals having the nominal composition $MnMg_5L_{12}$. Anal. Found (Calcd): Mn, 4.1(3.5); Mg, 7.8(7.7). IR (cm^{-1}, KBr pellet): 2963, 2932, 1618, 1491, 1429, 1318, 1219, 1089, 805. Compounds having different *n* values were prepared by the same method but by varying the ratio of Mn_6L_{12} to Mg_6L_{12} in the reaction mixture. All of the compounds gave essentially identical infrared spectra. Preparative and compositional data on these other materials are presented in Table 1.

Table 1. Compositional Data on $Mn_nMg_{6-n}(O_2CNEt_2)_{12}$ Complexes

nominal composition Mn_nMg_{6-n}[a]	n[b]	n[c]	x[d]	x[e]
Mn_6		6.0	0.007	0
Mn_5Mg_1	5.3	5.0	0.068	0.033
Mn_4Mg_2	4.1	4.1	0.14	0.12
Mn_3Mg_3	2.9	2.8	0.24	0.27
Mn_1Mg_5	1.1	1.1	0.63	0.70

[a] Based on the preparative ratio. [b] Determined from elemental microanalysis data on single crystals. [c] Determined from the slope of $1/\chi$ vs *T* plots. [d] Determined from the *y* intercept of the χT vs *T* plot, where *y* intercept/4.375 = *x*. [e] Determined from speciation equilibria and eq 1.

X-ray Crystallography. X-ray measurements on $MnMg_5L_{12}$ were made using a Bruker SMART APEX instrument with CCD detection. Cell refinement was accomplished using Saint 6.02. Structure solution utilized SHELXS-97, and refinement of F^2 against all reflections utilized SHELXL-97. The Mn/Mg occupancy in both metal ion sites was permitted to float independently. The general site yielded a Mn/Mg ratio of 0.2073(18)/0.7927(18), and the special site yielded a Mn/Mg ratio of 0.069(2)/0.931(2). This results in a net stoichiometry of $Mn_{0.97}Mg_{5.03}L_{12}$ determined from X-ray diffraction. The ethyl group represented by the C8−C9/C8′−C9′ pair is disordered in the ratio 0.886(9)/0.114(9), respectively. It should also be noted that the unusually large shift/esd ratio in the final refinement is due to the largest correlation matrix elements related to C8 and C8′. This is because C8 and C8′ occupy nearly the same space, and it was not possible for the refinement to settle uniquely. Details of X-ray data collection and refinement are presented in Table 2 and in the Supporting Information.

Results and Discussion

The structure of $MnMg_5L_{12}$ determined from single-crystal X-ray diffraction confirmed that the complex consists of discrete M_6L_{12} units, Figure 1, and is isostructural with previous materials of this structure type.[23−26] The molecular framework consists of six metal ions residing in two symmetry-inequivalent sites, indicated by the green and orange ellipsoids in Figure 1. The four terminal metal ions (orange) are pentacoordinate, and the ligand environment is best described as a distorted square pyramidal arrangement, as indicated by a value for the trigonality index $\tau = 0.40$.[27] The two central metal ions (green) are hexacoordinate but have a geometry highly distorted from octahedral. The coordination polyhedra of the metal ions are linked to form two intertwined trimeric units cross-linked by the diethyl carbamate ligands. This gives the molecular unit its characteristic helical D_2 symmetry. The space group is centrosymmetric because the unit cell consists of equal numbers of right-handed (Δ) and left-handed (Λ) helical configurations that are arranged in alternating layers related by a crystallographic inversion center.

From refinement of the X-ray data, we determined the mole fraction m_{penta} of Mn^{2+} in the pentacoordinate site to be 0.21 with the corresponding occupancy m_{hexa} in the

(26) Caudle, M. T.; Nieman, R. A.; Young, V. G. *Inorg. Chem.* **2001**, *40*, 1571−1575.

(27) Addison, A. W.; Rao, T. N.; Reedijk, J.; van Rijn, J.; Verschoor, G. C. *J. Chem. Soc., Dalton Trans.* **1984**, 1349−1356.

Table 2. Single-Crystal X-ray Diffraction Data Collection and Refinement for $MnMg_5(O_2CNEt_2)_{12}$

empirical formula	$C_{60}H_{120}Mn_{5.04}Mg_{0.96}N_{12}O_{24}$	temp (K)	298(2)
fw	1569.10	λ (Å)	0.71073
cryst size (mm)	0.22 × 0.18 × 0.08	no. of measured reflns	33519
cryst syst	orthorhombic	no. of independent reflns	3817
space group	Ccca	no. of obsd reflns	1824
color	colorless	R_{all}[a]	0.0962
a (Å)	20.6773(12)	R_{obsd}[a]	0.0459
b (Å)	25.2183(14)	wR_{all}[a]	0.1288
c (Å)	16.5171(9)	wR_{obsd}[a]	0.1137
V (Å^3)	8612.8(8)	GOF	0.839
Z	4		

[a] Refined on F_o^2.

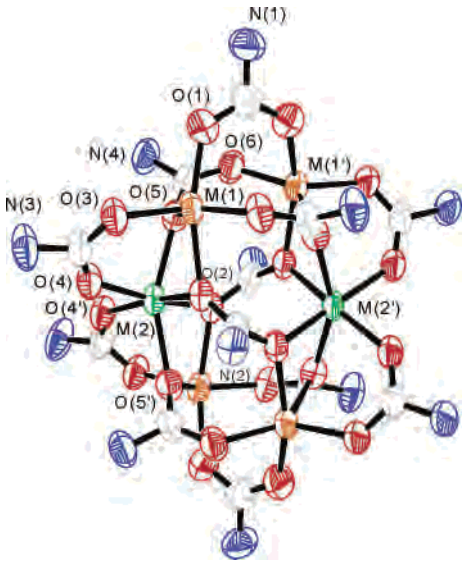

Figure 1. ORTEP drawing of the molecular unit in $MnMg_5L_{12}$ showing atomic positions in the M_6 core. Ethyl groups have been omitted for clarity. Only relevant symmetry-related atoms are labeled. The green ellipsoids represent the hexacoordinate sites, and the orange ellipsoids represent pentacoordinate sites. Bond lengths (Å): M(1)−O(1), 1.996(3); M(1)−O(2), 2.136(2); M(1)−O(3), 1.969(2); M(1)−O(5), 2.088(2); M(1)−O(6′), 2.011(2); M(2)−O(4), 2.022(2); M(2)−O(2), 2.087(2); M(2)−O(5), 2.174(2); M(1)···M(1′), 3.42; M(1)···M(2), 3.17; M(2)···M(2′), 4.48. Bond angles (deg): O(3)−M(1)−O(6′), 122.18(9); O(5)−M(1)−O(3), 98.32(9); O(5)−M(1)−O(6′), 137.32(8); O(1)−M(1)−O(2), 161.05(9); O(4)−M(2)−O(2), 85.93(7); O(4)−M(2)−O(4′), 87.48(12); O(5)−M(2)−O(5′), 155.44(10).

hexacoordinate site to be 0.069. The net doping factor $n = 4m_{penta} + 2m_{hexa} = 0.97$, which is in good agreement with $n = 1.1$ determined from compositional microanalysis and with $n = 1.05$ expected on the basis of the Mn/Mg ratio in the preparative reaction mixture. The fraction of Mn^{2+} in the hexacoordinate site is given by $2m_{hexa}/(4m_{penta} + 2m_{hexa}) = 0.14$, so that at low Mn/Mg ratios we generally expect about 14% of the total Mn^{2+} to reside in the hexacoordinate site. The data in Table 1 for *n* show that the experimentally determined composition is generally reflective of the composition of the reaction mixture, so that the preparative methodology we have developed permits rational synthesis of heteronuclear Mn/Mg complexes having any value for *n*.

The 3-fold larger Mn occupancy in the pentacoordinate site reveals a clear preference for the Mn^{2+} to reside in this site relative to the hexacoordinate site since the lack of a site preference would yield identical occupancies in both sites. The difference in relative site occupancy is informative regarding the nature of the metal ion distribution in the

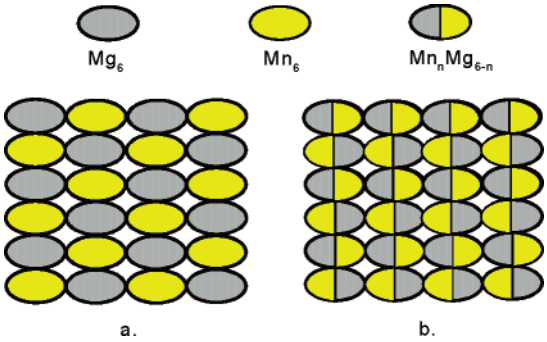

Figure 2. Schematic representation of metal ion mixing in M_6L_{12} at the crystallographic level (a) vs the molecular level (b).

crystal. A crystal consisting of randomly distributed but intact Mn_6L_{12} and Mg_6L_{12} units must show identical Mn occupancies in the two sites that reflect the net ratio Mn_6L_{12}/Mg_6L_{12}. Nonequivalent occupancies for the hexacoordinate and pentacoordinate sites can only arise from a differential distribution of Mn^{2+} ions within individual molecular units, which in turn can only result from net scrambling of metal ions between M_6L_{12} units. These two situations are illustrated schematically in Figure 2. State **a** represents the result of randomization of Mn^{2+} at a purely crystallographic level, without scrambling between molecular units. State **b** represents the result of additional randomization of Mn^{2+} at the molecular level. Even if the two states are enthalpically identical, state **b** has a larger number of statistical degrees of freedom. As a result, there is a driving force for randomization of state **a** to give state **b** that results from the entropy of mixing. If the Mn^{2+} distribution were entirely random, there would be no difference in pentacoordinate and hexacoordinate site occupancies and states **a** and **b** would not be distinguishable. The chemical basis for the metal ion site preference is not immediately obvious since the d^5 Mn^{2+} ion has a spherically symmetric electronic configuration and should exhibit no preference on the basis of ligand field energies. We showed previously that Co^{2+} resides exclusively in the pentacoordinate site,[23] which was ascribed to the more favorable ligand field energy of the d^7 ion in an idealized square pyramidal environment. The fact that 14% of the Mn^{2+} resides in the hexacoordinate site therefore may indicate the lack of ligand field energy in the present case. The ionic radii of Mn^{2+} (97 ppm) and Mg^{2+} (89 ppm) are different,[28] which might also account for the modest preference of the larger Mn^{2+} ion for the pentacoordinate site.

(28) Shannon, R. D. *Acta Crystallogr.* **1976**, *A32*, 751.

Scheme 1

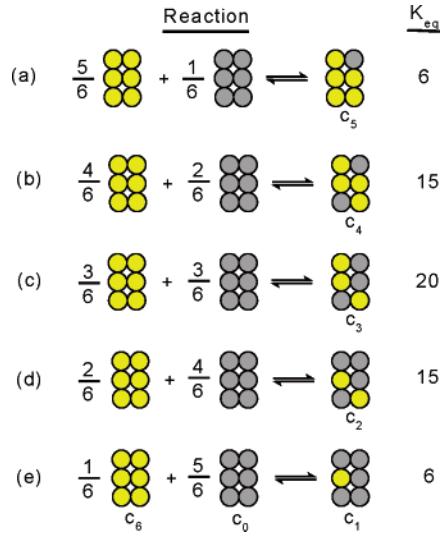

The interaction between Mn_6L_{12} and Mg_6L_{12} to give mixed-metal complexes can be modeled as a series of formation equilibria as shown in Scheme 1, where each circle represents a metal site in the complex and the yellow and gray shading indicates a site occupied by a Mn^{2+} or Mg^{2+} ion, respectively. We assume that there is a minimal enthalpic driving force for metal ion scrambling, and we make the approximation that Mn^{2+} ions are randomized between the hexacoordinate and pentacoordinate sites. Under these restrictions, the equilibrium constant for each reaction can be derived from a simple statistical accounting of the relative number of permutations in the reactant and product states. For example, there are six possible ways to construct the Mn_5MgL_{12} complex corresponding to the six possible sites in which the Mg ion might reside. There is only one possible permutation of the reactant state, so $K_{eq} = 6$, which is equal to the number of product permutations divided by the number of reactant permutations. The remaining K_{eq} values were determined accordingly. Scheme 1 yields a series of simultaneous equations relating the concentrations of each species, and these can be solved for any ratio of Mg to Mn to yield the normalized speciation diagram in Figure 3. This diagram models both solution and solid-state speciation in the $Mn_nMg_{6-n}L_{12}$ system, and thus provides a useful framework for understanding EPR and magnetic susceptibility data collected on these compounds. Most germane to the present study, the fraction x of Mn^{2+} in isolated sites can be determined from the speciation equilibria using eq 1. The

$$x = \frac{1}{[\mathrm{Mn}]_{\mathrm{tot}}}(c_1 + 0.60c_2 + 0.30c_3 + 0.13c_4) \qquad (1)$$

coefficients in eq 1 arise from the fact that, in molecular units having between two and four manganese ions, a fraction of configurations exist that isolate one or more ions, and these will also contribute to x, Scheme S1 in the Supporting Information.[29] Mn^{2+} ions are considered isolated if the Mn···Mn distance is greater than 4.0 Å and are considered coupled if the Mn···Mn distance is less than 3.5 Å. Values for x determined by inserting speciation data from Figure 3 into eq 1 are presented in Table 1.

(29) Deposited in the Supporting Information.

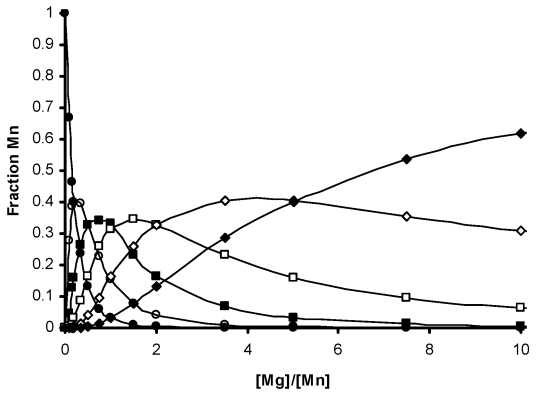

Figure 3. Speciation plot of the $Mn_6L_{12} + Mg_6L_{12}$ system showing the normalized fraction of manganese present in each molecular species. For each species $Mn_nMg_{6-n}L_{12}$, the fraction of Mn = $(nc_n)/[\mathrm{Mn}]_{\mathrm{tot}}$. Key: ●, Mn_6L_{12}; ○, Mn_5MgL_{12}; ■, $Mn_4Mg_2L_{12}$; □, $Mn_3Mg_3L_{12}$; ◇, $Mn_2Mg_4L_{12}$; ◆, $MnMg_5L_{12}$.

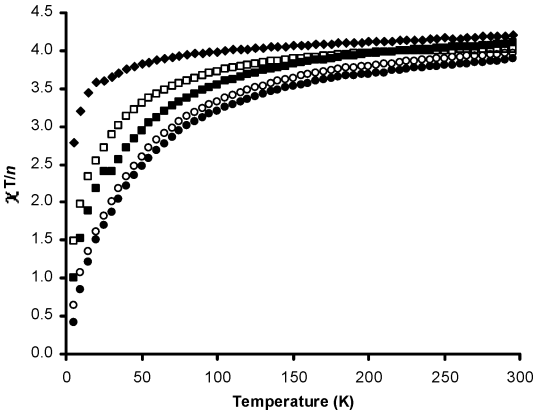

Figure 4. Magnetic susceptibility of $Mn_nMg_{6-n}L_{12}$ as a function of absolute temperature: ●, Mn_6L_{12}; ○, Mn_5MgL_{12}; ■, $Mn_4Mg_2L_{12}$; □, $Mn_3Mg_3L_{12}$; ◆, $MnMg_5L_{12}$.

Temperature-dependent magnetic susceptibility data for compounds $Mn_nMg_{6-n}L_{12}$ having different n values all exhibit Curie−Weiss behavior with linear plots of $1/\chi$ vs T.[29] For a multinuclear complex containing n d^5 metal ions, the slope of the $1/\chi$ vs T plot is given by $1/\alpha$, where α is given by eq 2.[30] A plot of α vs n gives an intercept of zero

$$\alpha = 4.375n \qquad (2)$$

and a slope of 4.40, demonstrating very good agreement with eq 2, Figure S1 in the Supporting Information.[29] Figure 4 shows plots of $\chi T/n$ as a function of temperature. The data for all complexes are consistent with antiferromagnetic coupling of the Mn^{2+} ions since $\chi T/n$ decreases monotonically with decreasing temperature. The net magnetic susceptibility χT is a weighted sum of the paramagnetism of isolated Mn^{2+} ions ($\chi_{\mathrm{isolated}}T$) and of the antiferromagnetism ($\chi_{\mathrm{coupled}}T$) from clusters of magnetically coupled Mn^{2+} ions, as shown by eq 3.

$$\chi T = (x)\chi_{\mathrm{isolated}}T + (1 - x)\chi_{\mathrm{coupled}}T \qquad (3)$$

In principle, eq 3 can be fit to the data in Figure 4 by

assuming Curie behavior for $\chi_{isolated}$ and a Heisenberg exchange Hamiltonian for $\chi_{coupled}$. Calculation of the former is straightforward, but calculation of $\chi_{coupled}$ presents a number of difficulties. Approaches do exist for the calculation of spin levels in polynuclear complexes including a number of hexanuclear architectures,[31] but this still remains an advanced problem, especially when more than one *J* coupling parameter must be included. In addition, the speciation diagram shows that a mixture of $Mn_nMg_{6-n}L_{12}$ species is present except under conditions where [Mg] is either large or very small. An exact solution to eq 3 would therefore require that each individual species present be treated. It is therefore unlikely that a rigorous analysis of the magnetic data in the context of eq 2/eq 3 would yield quantitatively meaningful values for *J* coupling parameters.

Equation 3 is qualitatively instructive in interpreting the normalized χT vs *T* plots in Figure 4, however. When [Mg] $\ll$ [Mn], Mn_6L_{12} is the dominant species, so *x* is near zero. In this case the net magnetic susceptibility is dominated by the temperature-dependent term $\chi_{coupled}T$. Since the ground state of an antiferromagnetically coupled Mn_6L_{12} complex has $S = 0$, χT extrapolates to zero as *T* approaches zero as shown by the closed circles. When [Mg] $\gg$ [Mn], $MnMg_5L_{12}$ dominates and *x* is near unity. Under these conditions, χT will be temperature-independent since $\chi T \approx \chi T_{isolated} = S(S + 1)Ng^2\beta^2/3k$. For intermediate cases where [Mg] is comparable to [Mn], a mixture of species exist and χT is the superposition of the temperature-dependent $\chi T_{coupled}$ arising from antiferromagnetically coupled polynuclear Mn^{2+} species and the temperature-independent $\chi T_{isolated}$ arising from magnetically isolated Mn^{2+} ions. As a result, the χT vs *T* plots do not extrapolate to zero at $T = 0$ except for low Mg^{2+} content samples, and the *y* intercept thus permits an estimate of *x*. These values compare favorably with *x* calculated using eq 1, Table 1. Thus, the magnetic data in Figure 4 show a continuum of magnetic behavior as a function of Mg^{2+} content, which is only consistent if metal ion scrambling results in generation of isolated Mn^{2+} ions.

The X-band EPR spectrum of Mn_6L_{12} at 100 K in frozen solution consists of a single broad signal centered at $g_{eff} = 2$, Figure 5a, which is consistent with weakly antiferromagnetically coupled Mn^{2+} ions. When a 100-fold excess of Mg_6L_{12} is added to a solution of Mn_6L_{12}, the spectrum changes dramatically, Figure 5b. The dominant signal now appears between 1400 and 2000 G, and at low temperature this signal shows hyperfine interactions absent in the original spectrum of Mn_6L_{12}. Control experiments show that Mg_6L_{12} exhibits no EPR signals by itself, indicating that it contains no Mn^{2+} impurities. Therefore, the new signals must arise from the interaction between Mg_6L_{12} and Mn_6L_{12}. As the temperature is decreased to 5 K, the spectrum above 2000 G broadens and a weak new signal appears at 800 G, Figure 5c. This latter signal exhibits a well-defined six-line hyperfine

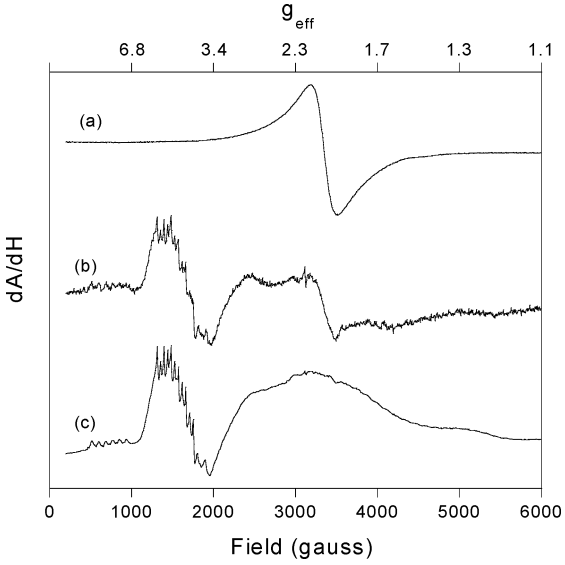

Figure 5. X-band (9.4 GHz) EPR spectra in frozen $CHCl_3$, 5.0 G field modulation amplitude, 100 kHz modulation frequency, 1024 data points collected: (a) 1 mM Mn_6L_{12}, $T = 100$ K, 2.0 mW power; (b) 1 mM Mn_6L_{12} + 100 mM $Mg_6(L)_{12}$, $T = 100$ K, 2.0 mW power; (c) 1 mM Mn_6L_{12} + 100 mM Mg_6L_{12}, $T = 5$ K, 1.0 mW power.

interaction, indicating that it arises from a spin-isolated Mn^{2+} ion with $g_{eff} = 8.3$. This is unlikely to be the result of decomposition to a mononuclear Mn^{2+} species since these typically exhibit a six-line signal at $g_{eff} = 2$ in the X-band spectrum. The 1400−2000 G signal exhibits a complex hyperfine structure consisting of a minimum of 13 lines, but the hyperfine spacing is not constant. Thus, it is unlikely that this signal arises from a single multinuclear Mn^{2+} center. Rather, the signal is more consistent with two or more overlapping six-line signals that arise from isolated Mn^{2+} ions. Spin isolation results when a molecular unit contains only a single Mn^{2+} ion or when it contains two Mn^{2+} ions in well-separated sites. In either case, formation of spin-isolated Mn^{2+} ions requires scrambling of individual Mn^{2+} and Mg^{2+} ions between the hexanuclear molecular units in solution. These data are therefore consistent with the magnetic data in demonstrating the net exchange of individual Mn^{2+} ions between hexanuclear clusters. This is also consistent with the speciation diagram, which shows that, under the conditions of the EPR experiment where Mn/Mg = 0.01, 95% of all of the Mn^{2+} exists as $MnMg_5L_{12}$, and by eq 1, 98% resides in isolated sites. We can therefore conclude that the EPR signals we observe originate from Mn^{2+} ions in these isolated sites.

Crystallization from a solution containing Mn_6L_{12} and Mg_6L_{12} in a 1/100 ratio gives single crystals of nominal composition $Mn_{0.06}Mg_{5.94}L_{12}$. The powder obtained by crushing a single crystal of this material gives the EPR spectrum shown at the top of Figure 6. It is qualitatively similar to the solution spectrum in showing a dominant multiline signal centered at about 1600 G, which shows well-resolved hyperfine structure in the powder spectrum. The intense signals in this range henceforth will be referred to collectively as the $g_{eff} = 4$ signals. The spectrum also exhibits a less intense group of signals spanning the entire field range up to 6000 G. These signals, referred to as the wide signals,

(30) Kahn, O. *Molecular Magnetism*; VCH Publishers Inc.: New York, 1993.

(31) Gatteschi, D.; Pardi, L. In *Research Frontiers in Magnetochemistry*; O'Connor, C. J., Ed.; World Scientific: River Edge, NJ, 1993. Caneschi, A.; Cornia, A.; Fabretti, A. C.; Foner, S.; Gatteschi, D.; Grandi, R.; Schenetti, L. *Chem.−Eur. J.* **1996**, *2*, 1379−1387.

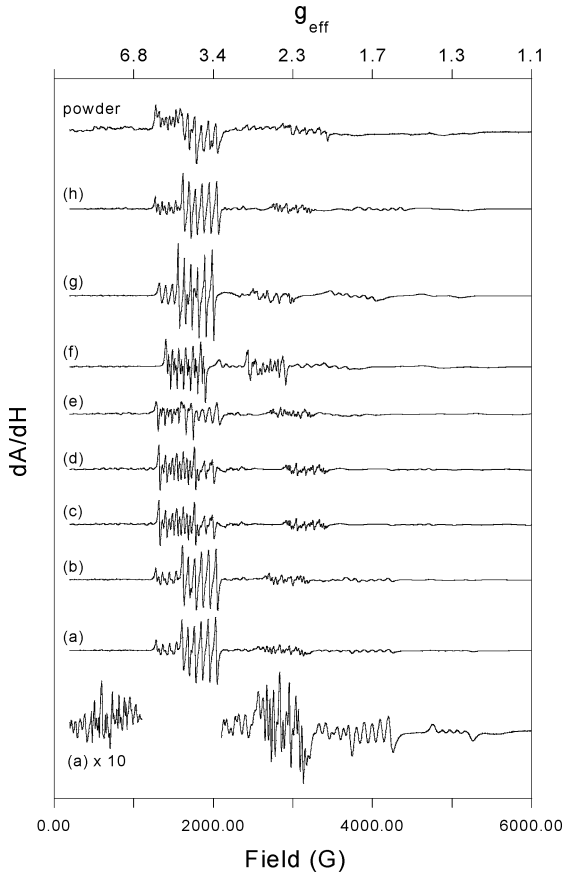

Figure 6. X-band (9.4 GHz) EPR spectra of $Mn_{0.06}Mg_{5.94}L_{12}$ in the solid state at 100 K, 10 mW power, 8.0 G field modulation, and 100 kHz modulation frequency. The single crystal is oriented with the long axis perpendicular to *H*. The angle ϕ corresponds to rotation about this axis. The initial orientation (a) is at arbitrary ϕ. Single-crystal spectra (b−h) were measured for values of ϕ relative to that of (a). Key: (a) $\phi = 0°$; (b) $\phi = 20°$; (c) $\phi = 40°$; (d) $\phi = 50°$; (e) $\phi = 60°$; (f) $\phi = 70°$; (g) $\phi = 80°$; (h) $\phi = 90°$. The powder spectrum was measured at 100 K, 1.0 mW power, 4.0 G field modulation, and 100 kHz modulation frequency.

show evidence of hyperfine interactions as well. The hyperfine structure in the $g_{eff} = 4$ and wide signals becomes even more resolved when a spectrum is measured on a single crystal, Figure 6a. This includes obvious six-line ^{55}Mn interactions at 1700 and 4000 G, which confirm that the Mn^{2+} ions are magnetically isolated in the solid state. Furthermore, the wide signal is resolved into discrete signals at 750, 2850, 3900, and 4950 G components in the single crystal, and the EPR absorbance spectrum indicates a fifth component of the wide signal that lies beneath the $g_{eff} = 4$ signals at about 1800 G. Thus, the solution-state, powder, and single-crystal EPR spectra are in agreement with the magnetic data in suggesting the formation of isolated Mn^{2+} ions from the reaction of Mn_6L_{12} with excess Mg_6L_{12}.

The single-crystal EPR spectrum exhibits a marked angular dependence as shown by Figure 6. This arises from the orthorhombic crystal structure in which each molecular unit has its long C_2 axis aligned parallel with the long axis of the unit cell. As the single crystal is rotated with respect to the field, changes in the $g_{eff} = 4$ signal occur with a periodicity of 90°, and this permits resolution of at least three distinct six-line components contributing to the spectrum in the $g_{eff} = 4$ region. The most intense of these is centered at 1813 G ($g_{eff} = 3.7$) with an 84 G hyperfine interaction. Two other signals are identified at 1620 ($g_{eff} = 4.1$) and 1540 ($g_{eff} = 4.3$) G with 87 and 90 G hyperfine interactions, respectively. The wide signal also changes upon reorientation in the magnetic field. Notably, the components at 2800 and 4000 G in Figure 6a migrate to higher field first and then to lower field as the crystal is rotated. The high-field and low-field signals at 5000 and 800 G also undergo a periodic change as a function of crystal orientation.

The EPR spectrum of $Mn_{0.06}Mg_{5.96}L_{12}$ can be qualitatively understood in the context of the spin Hamiltonian in eq 4, which neglects the nuclear hyperfine interactions. The

$$\mathbf{H} = g\beta H\cdot\mathbf{S} + D[S_z^2 - 0.33S(S+1)] + E[S_x^2 - S_y^2] \quad (4)$$

parameters *D* and *E* represent the axial and rhombic perturbation of the Zeeman term. If *D* and *E* are both zero, then the only contributor to the spectrum is the first-order Zeeman term and the result for Mn^{2+} is an isotropic spectrum with a single six-line signal with g_{eff} near 2.0. This is typical of manganese in highly cubic coordination environments and/or in weak ligand fields. Axial systems for which $E = 0$ but $0 < D \leq g\beta H$ show five equally spaced fine structure transitions separated in field by $H_i - H_{i-1} = 2D/g\beta$.[13] The components of the wide signal exhibit behavior consistent with $0 < D \leq g\beta H$. The average *H* spacing is 1050(71) G, giving $|D| = 0.05$ cm^{-1}, which is the zero-field splitting parameter for *H* parallel to the tetragonal axis. We cannot determine the sign of *D* from this analysis. A zero-field splitting parameter of this magnitude has been observed for carboxylatomanganese(II) complexes,[20,22] and is consistent with weak mixing of the $^6A_{1g}$ ground state with an $S = 3/2$ excited state. States of suitable A_1 symmetry arise directly from a cubic ligand field or from tetragonal splitting (D_{4h} or C_{4v}) of a high-energy ^4E_g state, as shown by the partial correlation diagram in Chart 1. However, even for strong tetragonal splitting the $^6A_1 \rightarrow {}^4A_1$ gap is large, resulting in poor overlap of these states and a small value for *D*. The *g* value derived from the $M_s = -1/2 \rightarrow +1/2$ transition is 2.2, which refers to the specific orientation of the field relative to the molecular axes, and is probably the result of an anisotropic **g** tensor in this system. The EPR signals are broadened in the powder spectrum, consistent with an angular dependence that arises from an anisotropic **g** tensor. This interpretation implies a weak axial ligand field of approximate D_{4h} or C_{4v} symmetry for the Mn^{2+} ions giving rise to these signals, which is most consistent with the pentacoordinate site in the complex, Figure 7a, where the unique axis lies along the Mn−O(3) vector.

Signals near $g_{eff} = 4$ arise in d^5 systems when *D* and *E* are both comparable to $g\beta H$. More specifically, it arises for rhombically distorted fields when $E/D \approx 1/3$, which is the case for a purely rhombic system ($E/D = 0$ for axial systems). This situation has been well-studied in Fe^{3+} systems but has not been as extensively examined in Mn^{2+} complexes. In this case, the primary contributor to the EPR spectrum is the middle Kramer's doublet arising from admixture of a *J*

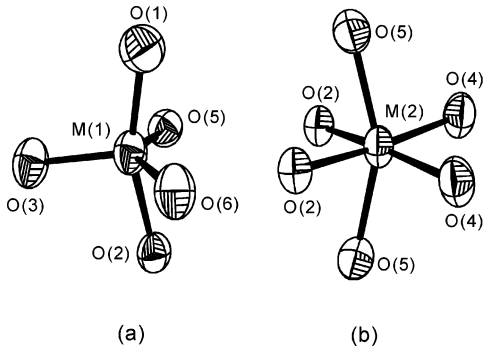

Figure 7. Coordination environments about metal sites M(2) (a) and M(1) (b). Refer to Figure 1 for bond lengths and angles.

Chart 1

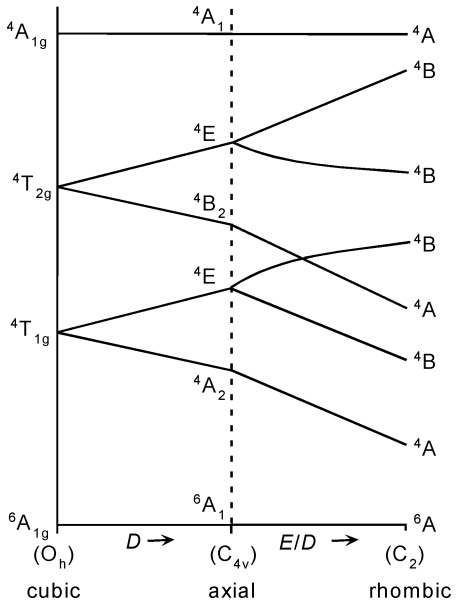

$= 5/2$ excited state into the $^6A_1$ ground state.[32] This type of spectrum requires that $D/h\nu > 1$, which means that, for the X-band regime, $|D| \geq 0.3$ cm^{-1}. D values in this range are regularly observed in high-spin Fe^{3+} and Mn^{2+} porphyrin complexes,[14−16] and in rhombic systems having local C_2 or D_2 symmetry imposed by relatively strong field ligands.[15] The larger zero-field splitting can be attributed to a low-lying ^4A excited state that can mix more effectively with the ^6A ground state in C_2-symmetric systems, Chart 1. This induces a larger value for D than in the preceding case and results in a nearly isotropic g value near 4.[32] The $g_{eff} = 4$ signals are therefore most consistent with a rhombic C_2 symmetric site, and are thus assigned as arising from the Mn^{2+} ions residing in the hexacoordinate site, Figure 7b, which has a local C_2 site symmetry. EPR signals near $g_{eff} = 4.3$ have been observed previously only in complexes having one or more medium-field to strong-field ligands,[16] so it is surprising that we observe this type of signal in the homoleptic carbamato system consisting entirely of weak-field ligands. The present data therefore indicate that weak-field ligands can have a substantial impact on the EPR spectroscopy of Mn^{2+} complexes if the structural distortion is sufficiently large.

The $g_{eff} = 4$ signals in the spectrum of $Mn_nMg_{6-n}L_{12}$ bear special comment in the context of the extensive literature relating to the EPR spectroscopy of the water-oxidizing manganese cluster in photosystem II. The cluster consists of four manganese ions that can be cycled through three stable oxidation states, S_0-S_3, followed by one unstable state, S_4.[10,33] Oxidation to this terminal state results in the evolution of oxygen. EPR signals have been observed for all of the stable S_n states, although only the S_0 and S_2 states exhibit a spectrum in the normal perpendicular mode X-band regime. Thus, these signals are often used to monitor the system when it is cycled through the S states by single flash illumination. Illumination of the resting state, S_1, results in oxidation by one electron to give the S_2 state, which typically exhibits a multiline feature at $g = 2$.[34−36] This is to be expected for an antiferromagnetically coupled manganese cluster having an odd number of electrons, where one expects a $g = 2$ signal to arise from the $S = 1/2$ ground state of the multinuclear system. However, under certain illumination conditions, an alternative signal appears at $g_{eff} = 4.1$,[35−37] and there was initially considerable speculation about the origin of this signal. While the results of the present study might lead to speculation that the $g_{eff} = 4.1$ signal in photosystem II arises from a mononuclear Mn^{2+} site, it was shown early on that addition of ammonia during illumination results in a $g = 4.1$ signal having at least 14 contributing hyperfine lines.[38] Thus, it could not arise from a mononuclear manganese center. A number of other experiments on the $g_{eff} = 4.1$ signal point to its origin in the $S = 3/2$ state of a Mn(IV) center[36] or the $S = 5/2$ excited spin states of an antiferromagnetically coupled manganese complex.[39] Comparison of the EPR data on photosystem II with the EPR spectra in Figures 5 and 6 therefore highlights the fact that very different manganese complexes utilizing different spin mech-

(32) Blumberg, W. E. In *Magnetic Resonance in Biological Systems*; Ehrenberg, A., Malmström, B. G., Vänngård, T., Eds.; Symposium Publications Division; Pergamon Press: Oxford, 1967; Vol. 9.

(33) Vrettos, J. S.; Brudvig, G. W. *Philos. Trans. R. Soc. London, Ser. B* **2002**, *357*, 1395−1405. Goussias, C.; Boussac, A.; Rutherford, A. W. *Philos. Trans. R. Soc. London, Ser. B* **2002**, *357*, 1369−1381. Renger, G. *Biochim. Biophys. Acta* **2001**, *1503*, 210−228.

(34) Abramowicz, D. A.; Dismukes, G. C. *Biochim. Biophys. Acta* **1984**, *765*, 318−328. Haddy, A.; Aasa, R.; Andreasson, L. E. *Biochemistry* **1989**, *28*, 6954−6959. Sivaraja, M.; Dismukes, G. C. *Isr. J. Chem.* **1988**, *28*, 103−108. Aasa, R.; Hansson, O.; Vaenngaard, T. *Prog. Photosynth. Res., Proc. Int. Congr. Photosynth., 7th* **1987**, *1*, 577−580. Hansson, O.; Andreasson, L. E. *Biochim. Biophys. Acta* **1982**, *679*, 261−268. Dismukes, G. C.; Siderer, Y. *Proc. Natl. Acad. Sci. U.S.A.* **1981**, *78*, 274−278.

(35) De Paula, J. C.; Beck, W. F.; Brudvig, G. W. *J. Am. Chem. Soc.* **1986**, *108*, 4002−4009. De Paula, J. C.; Innes, J. B.; Brudvig, G. W. *Biochemistry* **1985**, *24*, 8114−8120.

(36) Hansson, O.; Aasa, R.; Vaenngaard, T. *Biophys. J.* **1987**, *51*, 825−832.

(37) Andreasson, L. E.; Hansson, O.; Von Schenck, K. *Biochim. Biophys. Acta* **1988**, *936*, 351−360. Cole, J.; Yachandra, V. K.; Guiles, R. D.; McDermott, A. E.; Britt, R. D.; Dexheimer, S. L.; Sauer, K.; Klein, M. P. *Biochim. Biophys. Acta* **1987**, *890*, 395−398. Ono, T.; Zimmermann, J. L.; Inoue, Y.; Rutherford, A. W. *Biochim. Biophys. Acta* **1986**, *851*, 193−201. Zimmermann, J. L.; Rutherford, A. W. *Biochemistry* **1986**, *25*, 4609−4615. Casey, J. L.; Sauer, K. *Biochim. Biophys. Acta* **1984**, *767*, 21−28.

(38) Kim, D. H.; Britt, R. D.; Klein, M. P.; Sauer, K. *J. Am. Chem. Soc.* **1990**, *112*, 9389−9391.

(39) Haddy, A.; Dunham, W. R.; Sands, R. H.; Aasa, R. *Biochim. Biophys. Acta* **1992**, *1099*, 25−34.

anisms can give rise to compelling similar EPR spectra. As a result, some care must be utilized when using EPR as a fingerprint for the structure and oxidation state in manganese-containing complexes and proteins.

Summary

Reaction between the isostructural hexanuclear Mn_6L_{12} and Mg_6L_{12} complexes results in scrambling of metal ions and formation of mixed complexes of the form $Mn_nMg_{6-n}L_{12}$. At sufficiently low doping factor n, magnetic susceptibility measurements show that this gives Mn^{2+} ions that are magnetically isolated from other Mn^{2+} ions. The solution and solid-state EPR spectra give a sharp and intense set of $g_{eff} = 4$ signals and a broad and less intense set of signals from 200 to 6000 G. These are ascribed to the Mn^{2+} ions residing in the hexacoordinate and pentacoordinate sites, respectively. The EPR spectrum was qualitatively explained in terms of the ligand field geometry around the two different sites. This system appears to be a rare example of how distortion in a weak ligand field can profoundly influence the EPR spectrum of molecular Mn^{2+} complexes. It is therefore germane in the context of the large body of EPR spectroscopic data on manganese proteins. The unique $g_{eff} = 4$ signals were discussed in the context of the EPR spectroscopy on the tetramanganese water-oxidizing complex of photosystem II.

Acknowledgment. Financial support from the National Science Foundation (Grant CHM 9985266 to M.T.C.) is appreciated. C.K.M. acknowledges the NSF for an REU fellowship.

Supporting Information Available: Scheme S1, Figure S1, and X-ray crystallographic data in CIF format for $MnMg_5L_{12}$. This material is available free of charge via the Internet at http://pubs.acs.org.

IC0349757